JOURNAL OF GUIDANCE, CONTROL, AND DYNAMICS
Vol. 17, No. 6, November–December 1994

Multivariable Stability and Robustness of Sequentially Designed Feedback Systems

Brett Newman*
Old Dominion University, Norfolk, Virginia 23529-0247
and
David K. Schmidt†
University of Maryland, College Park, Maryland 20742-3015

In sequential loop closure, the importance of evaluating the stability and stability robustness at the intermediate loop closures is well known. However, knowledge concerning how the intermediate loop closures, as well as the final loop closures, contribute to the stability and stability robustness of the overall feedback system holds special significance to the analysis and design of multivariable feedback systems. An analysis of the complete feedback system reveals the multivariable Nyquist contributions from the intermediate loop closures. It is also shown that the results greatly simplify if frequency separation exists between the intermediate loops. The analysis is presented with a two-step loop closure procedure using "inner" and "outer" loops that can be generalized to multistep situations. The control of the longitudinal dynamics of an aircraft is addressed to further clarify and demonstrate the results.

Introduction

CONSIDER the generic multivariable feedback loop in Fig. 1 with responses $y(s)$, control inputs $u(s)$, response commands $y_c(s)$, plant transfer function matrix $G(s)$, and compensator transfer function matrix $K(s)$. Typically, the compensator must stabilize all unstable modes present in the plant. Further, the compensator must ensure this stability in the presence of plant modeling errors.

Frequency-domain criteria for stability and stability robustness such as multivariable Nyquist stability and singular-value robustness theory are well known and extensively documented.[1–5] These tools are directly applicable to a given multivariable compensator in the format of Fig. 1. For example, closed-loop stability is indicated by the Nyquist diagram corresponding to $\det[I + KG]$. Further, stability robustness can be assessed by considering $\det[I + KG]$ or the singular-value trace corresponding to $\underline{\sigma}[I + KG]$. However, if the compensator is developed with a sequential loop closure strategy,[6,7] a void exists in the relationship between stability and stability robustness indicated after each loop closure and the stability and stability robustness of the complete feedback system.

For example, consider the two-step loop closures shown in Figs. 2 and 3, where the "inner loops" consist of outputs y_i and the "outer loops" consist of outputs y_o. It is important to observe here that the inner and outer loops can be multivariable. Further, observe that the block-diagram structure in Fig. 2 can be manipulated into the more classical looking inner and outer loop structure depicted in Fig. 4 if $K_i(s)$ and $G_i(s)$ are nonsingular. However, for ease of exposition the structure of Fig. 2 will be considered. With only the inner loops closed, system stability and robustness are indicated by the Nyquist diagram corresponding to $\det[I + K_iG_i]$ or the singular-value diagram corresponding to $\underline{\sigma}[I + K_iG_i]$. After the outer loops are closed, system stability and robustness are indicated by the Nyquist diagram or the singular-value diagram corresponding to $\det[I + K_oG_o']$ and $\underline{\sigma}[I + K_oG_o']$, respectively, where $G_o'(s)$ is the effective plant for the outer loop closure. How these intermediate characteristics relate to the overall system characteristics is of concern.

Although somewhat related, the singular perturbation literature[8–12] concerning feedback control applications typically emphasizes nominal stability concerns only, or robustness to model simplification errors exclusively, using some form of modern, multivariable control scheme formulated in the time domain. Further, central to singular perturbation theory is the development of original-system characteristics by studying the simplified system. Here, a classical, frequency-domain formulation making use of fundamental Nyquist stability theory without turning to simplified models is desired and stressed. Recent work dealing with two-scale systems in the frequency domain is also related to the work here.[13–16] However, the analysis presented here does not require frequency separation assumptions and is formulated more directly to classical robustness theory and its multivariable generalizations. The goal of this paper is to relate the stability and stability robustness evaluated at each stage of the (multivariable) sequential loop closure to that of the final feedback system, so as to offer insight into the analysis and design of sequentially developed feedback systems, and to suggest a multivariable extension to this frequently used classical synthesis technique.[17]

Multivariable Stability and Stability Robustness

Stability of the closed-loop system in Fig. 1 is completely determined by the roots of the closed-loop characteristic polynomial $\phi_{cl}(s)$. The closed-loop characteristic polynomial is related to the open-loop characteristic polynomial $\phi_{ol}(s)$ by the well-known relationship[18]

$$\frac{\phi_{cl}(s)}{\phi_{ol}(s)} = \det[I + K(s)G(s)] \tag{1}$$

Application of the principle of the argument[19] to Eq. (1) yields

$$N(0, \det[I + K(S)G(S)], C_{RHP}) = Z - P \tag{2}$$

where the notation $N(0, \det[I + KG], C_{RHP})$ denotes the number of encirclements of the origin made by the Nyquist diagram (i.e., the mapping of $\det[I + KG]$ as s traverses the contour C_{RHP}, which encloses the entire right-half of the complex plane). Further, Z is

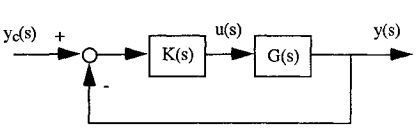

Fig. 1 Generic feedback loop.

Presented as Paper 91-2771 at the AIAA Guidance, Navigation, and Control Conference, New Orleans, LA, Aug. 12–14, 1991; received June 29, 1993; revision received Jan. 12, 1994; accepted for publication Jan. 18, 1994.

*Assistant Professor, Department of Aerospace Engineering. Member AIAA.

†Chairman and Professor, Department of Aerospace Engineering. Associate Fellow AIAA.

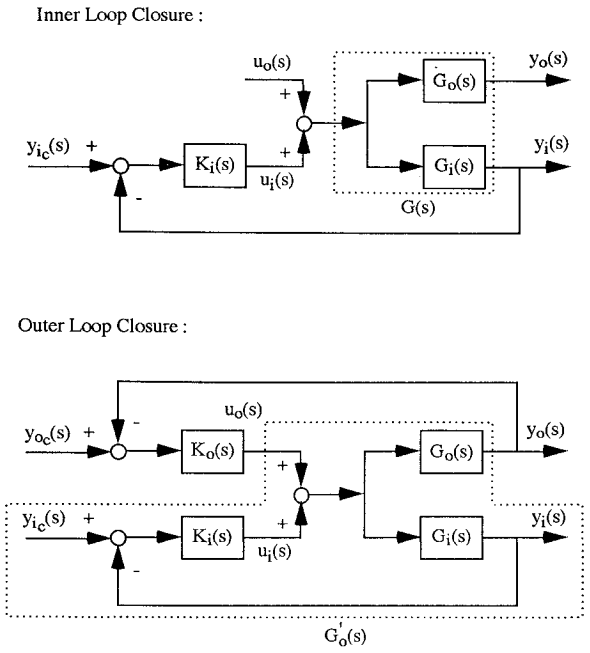

Fig. 2 Two-step loop closure with one input.

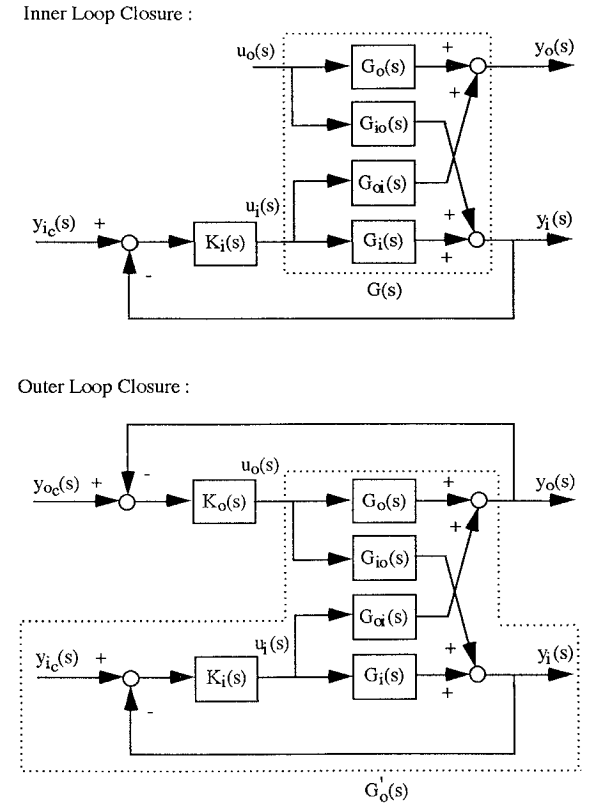

Fig. 3 Two-step loop closure with two inputs.

the number of closed-loop poles [roots of $\phi_{cl}(s)$] inside C_{RHP} and P is the number of open-loop poles [roots of $\phi_{ol}(s)$] inside C_{RHP}. For closed-loop asymptotic stability, no closed-loop poles may lie in the right-half plane, or

$$Z = 0 \Rightarrow N = -P \tag{3}$$

In other words, the Nyquist diagram must have the correct number of encirclements of the origin, namely, $-P$.

The feedback loop in Fig. 1 must also maintain stability in the presence of plant modeling errors. One common way to represent this error is with additive error $\Delta G(s)$ defined by

$$\Delta G(s) = G_T(s) - G(s) \tag{4}$$

where $G_T(s)$ denotes the "true" linear plant.

For the true feedback system, Eq. (1) becomes

$$\frac{\phi_{cl,T}(s)}{\phi_{ol,T}(s)} = \det[I + K(s)G_T(s)] \tag{5}$$

where $\phi_{cl,T}(s)$ and $\phi_{ol,T}(s)$ denote the true system's closed-loop and open-loop characteristic polynomials, respectively. Application of the principle of the argument[19] to Eq. (5) yields

$$N_T(0, \det[I + K(s)G_T(s)], C_{RHP}) = Z_T - P_T \tag{6}$$

where $N_T(0, \det[I + KG_T], C_{RHP})$ denotes the number of encirclements of the origin made by the true system's Nyquist diagram, Z_T is the number of true closed-loop poles in the right-half plane, and P_T is the number of true open-loop poles in the right-half plane. For closed-loop asymptotic stability of the true system, none of its closed-loop poles may lie in the right-half plane, or

$$Z_T = 0 \Rightarrow N_T = -P_T \tag{7}$$

It can be shown[4,5] that if 1) the nominal closed-loop system is asymptotically stable, or $N = -P$ [see Eq. (3)], and 2) the required number of encirclements of the origin is the same for both nominal and true closed-loop systems, or $P = P_T$ [see Eqs. (3) and (7)], then a necessary and sufficient condition guaranteeing closed-loop asymptotic stability of the true system is

$$\det[I + K(s)G(s, \varepsilon)] \neq 0, \qquad s \in C_{RHP}, \qquad 0 \leq \varepsilon \leq 1 \tag{8}$$

where $G(s, \varepsilon)$ is given as

$$G(s, \varepsilon) = G(s) + \varepsilon \Delta G(s) \tag{9}$$

Note that $\varepsilon = 0$ and $\varepsilon = 1$ correspond to the nominal and true plants, respectively. The geometric concept associated with Eq. (8) is that under assumptions 1 and 2, if the number of encirclements of the origin remains unchanged as the nominal Nyquist diagram is continuously warped to the shape of the true Nyquist diagram, then closed-loop asymptotic stability of the true system is assured. In other words, to maintain stability in the presence of modeling errors, the mapping $\det[I + K(s)G(s, \varepsilon)]$, $s \in C_{RHP}$, $0 \leq \varepsilon \leq 1$, must not pass through the origin.

A sufficient condition, developed from Eq. (8), guaranteeing true closed-loop asymptotic stability is[3-5]

$$\underline{\sigma}[I + K(j\omega)G(j\omega)] > \bar{\sigma}[K(j\omega)\Delta G(j\omega)] \quad \text{for } 0 \leq \omega \leq \infty \tag{10}$$

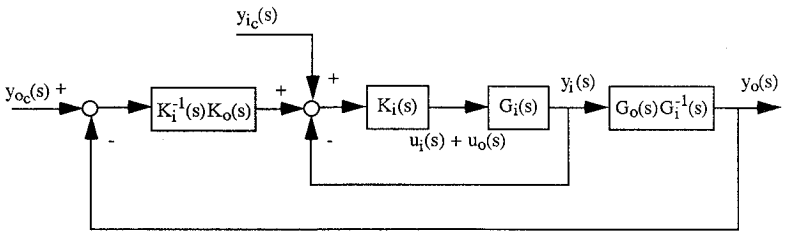

Fig. 4 Classical inner and outer loop structure.

If it is more appropriate to describe the plant modeling errors with multiplicative error (i.e., $G_T = G\{I + E\}$), then $G(s, \varepsilon)$ becomes

$$G(s, \varepsilon) = G(s)[I + \varepsilon E(s)] \tag{11}$$

and another sufficient condition guaranteeing true closed-loop stability is[3–5]

$$\underline{\sigma}[I + \{K(j\omega)G(j\omega)\}^{-1}] > \bar{\sigma}[E(j\omega)] \qquad \text{for } 0 \leq \omega \leq \infty \tag{12}$$

Sequential Loop Closure

Sequential loop closure is defined here as the use of any appropriate synthesis technique to design loops in stages to yield the final multivariable control law. For example, classical control techniques can be used to close scalar loops one at a time, or modern multivariable control techniques can be used in stages. In this approach, care must be taken because the selection and closure of a specific loop can both adversely affect the stability and performance already designed into previously closed loops and influence the stability and performance in subsequent loops yet to be closed. Thus, the key to success is the selection and order of the loop closure, and this is typically based upon a fundamental understanding of the plant dynamics. Specific examples of this approach can be found in Refs. 6 and 20–26. One situation where sequential loop closure is particularly effective is where frequency separation exists between each set of loops. In this particular but common situation most modern multivariable synthesis methods would lead to undesirable results if used to close *all* loops simultaneously. This is due to the fact that the loop transfers are forced to be closely spaced at crossover, which yields strong coupling and destroys any frequency separation naturally present.

The direct application of multivariable stability and stability robustness theory to the complete feedback system in Fig. 2 or 3 offers very little information about the stability and stability robustness at each loop closure step, which is of paramount importance during the synthesis. To obtain this information, the stability theory will be applied at each step in the loop closure process. First, however, it will be shown that the block-diagram structures in Figs. 2 and 3 are special cases of the structure in Fig. 1.

Consider the following partition of the system in Fig. 1, or

$$y(s) = \begin{bmatrix} y_1(s) \\ y_2(s) \end{bmatrix} \qquad y_c(s) = \begin{bmatrix} y_{1c}(s) \\ y_{2c}(s) \end{bmatrix} \qquad u(s) = \begin{bmatrix} u_1(s) \\ u_2(s) \end{bmatrix}$$

$$K(s) = \begin{bmatrix} K_{11}(s) & K_{12}(s) \\ K_{21}(s) & K_{22}(s) \end{bmatrix} \qquad G(s) = \begin{bmatrix} G_{11}(s) & G_{12}(s) \\ G_{21}(s) & G_{22}(s) \end{bmatrix}$$

$$\Delta G(s) = \begin{bmatrix} \Delta G_{11}(s) & \Delta G_{12}(s) \\ \Delta G_{21}(s) & \Delta G_{22}(s) \end{bmatrix} \tag{13}$$

$$G(s, \varepsilon) = \begin{bmatrix} G_{11}(s, \varepsilon) & G_{12}(s, \varepsilon) \\ G_{21}(s, \varepsilon) & G_{22}(s, \varepsilon) \end{bmatrix}$$

The block-diagram structure in Fig. 2 is obtained by selecting

$$\begin{aligned} K_{21}(s) &= 0 & K_{22}(s) &= 0 \\ G_{12}(s) = \Delta G_{12}(s) &= 0 & G_{22}(s) = \Delta G_{22}(s) &= 0 \end{aligned} \tag{14}$$

along with elimination of the zero columns and rows of $K(s)$, $G(s)$, and $\Delta G(s)$, leading to

$$\begin{aligned} K(s) &= [K_i(s)K_o(s)] & G(s) &= \begin{bmatrix} G_i(s) \\ G_o(s) \end{bmatrix} \\ \Delta G(s) &= \begin{bmatrix} \Delta G_i(s) \\ \Delta G_o(s) \end{bmatrix} & G(s, \varepsilon) &= \begin{bmatrix} G_i(s, \varepsilon) \\ G_o(s, \varepsilon) \end{bmatrix} \end{aligned} \tag{15}$$

The block-diagram structure in Fig. 3 is obtained by selecting

$$K_{12}(s) = 0 \qquad K_{21}(s) = 0 \tag{16}$$

leading to

$$K(s) = \begin{bmatrix} K_i(s) & 0 \\ 0 & K_o(s) \end{bmatrix} \qquad G(s) = \begin{bmatrix} G_i(s) & G_{io}(s) \\ G_{oi}(s) & G_o(s) \end{bmatrix}$$

$$\Delta G(s) = \begin{bmatrix} \Delta G_i(s) & \Delta G_{io}(s) \\ \Delta G_{oi}(s) & \Delta G_o(s) \end{bmatrix} \tag{17}$$

$$G(s, \varepsilon) = \begin{bmatrix} G_i(s, \varepsilon) & G_{io}(s, \varepsilon) \\ G_{oi}(s, \varepsilon) & G_o(s, \varepsilon) \end{bmatrix}$$

Stability at Each Loop Closure

Let P_K and P_G denote the number of poles of $K(s)$ and $G(s)$, respectively, in the right-half plane, or

$$P = P_K + P_G \tag{18}$$

Here P_K can be separated into the number of compensator poles in the right-half plane due to the inner loop compensation P_{K_i} and due to the outer loop compensation P_{K_o}, or

$$P_K = P_{K_i} + P_{K_o} \tag{19}$$

Further, P_G can be separated into the number of plant poles in the right-half plane to be stabilized with the inner loop P_{G_i} and with the outer loop $P_{G'_o}$, or

$$P_G = P_{G_i} + P_{G'_o} \tag{20}$$

Applying Nyquist theory to the inner loop closure yields

$$N_i(0, \det[I + K_i(s)G_i(s)], C_{\text{RHP}}) = Z_i - P_i \tag{21}$$

where $N_i(0, \det[I + K_iG_i], C_{\text{RHP}})$ denotes the number of encirclements of the origin made by the inner loop Nyquist diagram, Z_i is the number of closed-loop poles of the inner loop system in the right-half plane, and P_i is the number of open-loop poles of the inner loop system in the right-half plane. Although closed-loop stability of the complete feedback system is ultimately desired, requiring $Z_i = 0$ at this loop closure step is not necessary because the unstable poles represented by Z_i are to be stabilized by the outer loop. Using the notation in Eqs. (18–20), Z_i and P_i are given as

$$Z_i = P_{G'_o} \qquad P_i = P_{K_i} + P_G \tag{22}$$

and the encirclement requirement in Eq. (21) becomes

$$N_i = -P_{K_i} - P_{G_i} \tag{23}$$

Next, applying Nyquist theory to the outer loop closure yields

$$N_o(0, \det[I + K_o(s)G'_o(s)], C_{\text{RHP}}) = Z_o - P_o \tag{24}$$

where $N_o(0, \det[I + K_oG'_o], C_{\text{RHP}})$ denotes the number of encirclements of the origin made by the outer loop Nyquist diagram, Z_o is the number of closed-loop poles of the outer loop system in the right-half plane, and P_o is the number of open-loop poles of the outer loop system in the right-half plane. Since this is the last loop closure, the requirement

$$Z_o = 0 \Rightarrow N_o = -P_o \tag{25}$$

is necessary for asymptotic stability of the complete system. Using the notation in Eqs. (18–20), P_o is given as

$$P_o = P_{K_o} + P_{G'_o} \tag{26}$$

and the encirclement requirement in Eq. (25) becomes

$$N_o = -P_{K_o} - P_{G'_o} \tag{27}$$

In summary, for closed-loop asymptotic stability of the complete feedback system, the inner and outer loop Nyquist diagrams must have the correct number of encirclements of the origin, namely $-P_{K_i} - P_{G_i}$ and $-P_{K_o} - P_{G'_o}$, respectively.

There are practical control design problems where the inner loop closure results in the destabilization or stabilization of an open-loop mode associated with the outer loop. Note that the development given above does not consider this situation. To account for this, Z_i in Eq. (22) can be altered to $Z_i = P_{G'_o} + P^*$ where P^* represents the change in the number of remaining unstable poles after the inner loop closure. Positive P^* denotes destabilization while negative P^* denotes stabilization.

To understand how the inner and outer loop encirclement requirements relate to the encirclement requirement for the overall feedback system in Fig. 1, consider $\det[I + KG]$ and the partitioning in Eq. (13), or

$$\det[I + KG] = \det\begin{bmatrix} I + K_{11}G_{11} + K_{12}G_{21} & K_{11}G_{12} + K_{12}G_{22} \\ K_{21}G_{11} + K_{22}G_{21} & I + K_{21}G_{12} + K_{22}G_{22} \end{bmatrix} \quad (28)$$

Using the identity for the determinate of a partitioned matrix[27] yields

$$\begin{aligned} \det[I + KG] &= \det[I + K_{11}G_{11} + K_{12}G_{21}] \\ &\times \det[I + K_{21}G_{12} + K_{22}G_{22} \\ &- (K_{21}G_{11} + K_{22}G_{21})(I + K_{11}G_{11} + K_{12}G_{21})^{-1} \\ &\times (K_{11}G_{12} + K_{12}G_{22})] \end{aligned} \quad (29)$$

For the block-diagram structure in Fig. 2, Eq. (29) reduces to

$$\det[I + KG] = \det[I + K_iG_i]\det[I + K_oG_o(I + K_iG_i)^{-1}] \quad (30)$$

Observe from Fig. 2 that the effective transfer function between $y_o(s)$ and $u_o(s)$ with the inner loop closed is

$$G'_o = G_o(I + K_iG_i)^{-1} \quad (31)$$

Therefore, the result in Eq. (30) becomes

$$\det[I + KG] = \det[I + K_iG_i]\det[I + K_oG'_o] \quad (32)$$

On the other hand, for the block diagram in Fig. 3, Eq. (29) reduces to

$$\begin{aligned} \det[I + KG] &= \det[I + K_iG_i] \\ &\times \det[I + K_o\{G_o - G_{oi}(I + K_iG_i)^{-1}K_iG_{io}\}] \end{aligned} \quad (33)$$

From Fig. 3 note that the effective transfer function between $y_o(s)$ and $u_o(s)$ with the inner loop closed is

$$G'_o = G_o - G_{oi}(I + K_iG_i)^{-1}K_iG_{io} \quad (34)$$

Thus, Eq. (33) also becomes identical to Eq. (32).

The result in Eq. (32) is the key to relating the encirclement requirement at each step to the encirclement requirement for the complete feedback system. Using the conformal mapping identity for the product of two functions,[19] Eq. (32) yields

$$N = N_i + N_o \quad (35)$$

Thus, the number of encirclements of the origin made by the Nyquist diagram for the complete feedback loop equals the sum of the number of encirclements for the inner and outer loop systems. Each loop closure contributes to the "unwrapping" of the origin. Further, by substituting Eqs. (23) and (27) into Eq. (35), it can be seen that closed-loop asymptotic stability, as indicated by Eq. (3), is implied if the individual encirclement requirements for the inner and outer loop systems are achieved.

Just as in the case of single-loop closures, Eq. (32) can also be used to relate the Nyquist diagram at each "multivariable" step to the Nyquist diagram for the complete feedback system. Any point on a Nyquist diagram is a complex number with magnitude and phase. Thus, if one defines

$$\begin{aligned} \det[I + K(j\omega)G(j\omega)] &= Me^{j\theta} \\ \det[I + K_i(j\omega)G_i(j\omega)] &= M_ie^{j\theta_i} \\ \det[I + K_o(j\omega)G'_o(j\omega)] &= M_oe^{j\theta_o} \end{aligned} \quad (36)$$

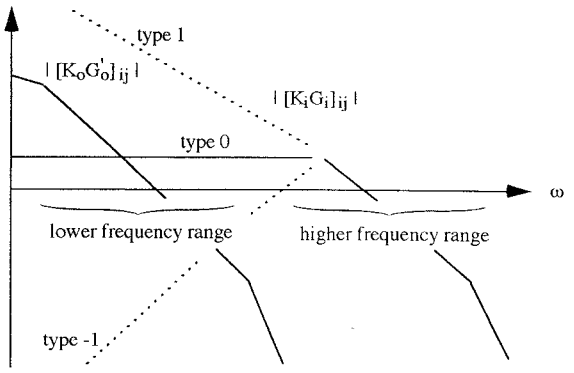

Fig. 5 Inner and outer system loop shapes.

the magnitude and phase contributions from the inner and outer loop Nyquist diagrams to the complete Nyquist diagram are

$$M = M_iM_o \qquad \theta = \theta_i + \theta_o \quad (37)$$

One common situation where matters are simplified is with frequency separation between the inner and outer loops. Suppose the inner loop crossover frequencies are in a higher frequency range and the outer loop crossovers all lie in a lower frequency range. Further, suppose the inner and outer loop shapes are as shown in Fig. 5, where both loops are well attenuated above their respective crossover and the inner loop system is type 1, 0, or -1 (Ref. 28).

For frequencies well above the outer loop crossover

$$|[K_o(j\omega)G'_o(j\omega)]_{ij}| \ll 1 \quad (38)$$

and Eq. (32) becomes

$$\det[I + KG] \approx \det[I + K_iG_i] \quad (39)$$

indicating the Nyquist diagrams for the complete feedback system and the inner loop system are approximately identical. On the other hand, for frequencies well below the inner loop crossover

$$\begin{aligned} \left|[K_i(j\omega)G_i(j\omega)]_{ij}\right| &\approx \left|\frac{1}{j\omega}[\overline{K_iG_i}(0)]_{ij}\right| \quad \text{for type 1 inner loop} \\ \left|[K_i(j\omega)G_i(j\omega)]_{ij}\right| &\approx \left|[K_i(0)G_i(0)]_{ij}\right| \quad \text{for type 0 inner loop} \\ \left|[K_i(j\omega)G_i(j\omega)]_{ij}\right| &\approx \left|j\omega[\overline{K_iG_i}(0)]_{ij}\right| \quad \text{for type } -1 \text{ inner loop} \end{aligned} \quad (40)$$

where $\overline{K_iG_i}(j\omega)$ is the remainder left over after $1/j\omega$ or $j\omega$ is factored from $K_i(j\omega)G_i(j\omega)$. With this, Eq. (32) becomes

$$\begin{aligned} \det[I + K(j\omega)G(j\omega)] &\approx \det\left[\frac{1}{j\omega}\overline{K_iG_i}(0)\right] \\ &\times \det[I + K_o(j\omega)G'_o(j\omega)] \quad \text{for type 1 inner loop} \\ \det[I + K(j\omega)G(j\omega)] &\approx \det[I + K_i(0)G_i(0)] \\ &\times \det[I + K_o(j\omega)G'_o(j\omega)] \quad \text{for type 0 inner loop} \\ \det[I + K(j\omega)G(j\omega)] &\approx \det[I + K_o(j\omega)G'_o(j\omega)] \\ &\quad \text{for type } -1 \text{ inner loop} \end{aligned} \quad (41)$$

indicating the Nyquist diagrams for the complete feedback system and the outer loop system are approximately identical for type -1 inner loop, different by only a constant scale factor for type 0 inner loop, and different by a frequency-dependent scale factor for type 1 inner loop.

Stability Robustness at Each Loop Closure

Let P_{G_T} denote the number of poles of the true plant $G_T(s)$ in the right-half plane, or

$$P_T = P_K + P_{G_T} \quad (42)$$

Here P_{G_T} can be separated into the number of true plant poles in the right-half plane to be stabilized with the inner loop $P_{G_{i,T}}$ and with the outer loop, $P_{G'_{o,T}}$, or

$$P_{G_T} = P_{G_{i,T}} + P_{G'_{o,T}} \tag{43}$$

Applying Nyquist theory after the inner loop closure around the true plant yields

$$N_{i_T}(0, \det[I + K_i(s)G_{i_T}(s)], C_{\text{RHP}}) = Z_{i_T} - P_{i_T} \tag{44}$$

where the notation is as before with the additional subscript T denoting consideration of the true system. Again, requiring $Z_{i_T} = 0$ at this loop closure step is not necessary. Using the notation in Eqs. (19), (42), and (43), Z_{i_T} and P_{i_T} are given as

$$Z_{i_T} = P_{G'_{o,T}} \qquad P_{i_T} = P_{K_i} + P_{G_T} \tag{45}$$

and the encirclement requirement in Eq. (44) becomes

$$N_{i_T} = -P_{K_i} - P_{G_{i,T}} \tag{46}$$

In a strict sense, if there are unstable modes still present after the nominal inner loop closure, stability robustness is undefined and the standard multivariable stability robustness theory is not applicable. In other words, the concept of how far the system is from instability is meaningless because the system is already unstable. What is required is a reinterpretation of the standard theory, and this is considered next.

Using the mechanics of the standard theory, if 1) the nominal inner closed-loop system satisfies the encirclement requirement $N_i = -P_{K_i} - P_{G_i}$ [see Eq. (23)] and 2) the required number of encirclements of the origin is the same for both nominal and true inner closed-loop systems, or $P_{G_i} = P_{G_{i,T}}$ [see Eqs. (23) and (46)], then inclusion of the modeling error $\Delta G_i(s)$ is guaranteed not to change the number of unstable poles when only the inner loop is closed if

$$\det[I + K_i(s)G_i(s, \varepsilon)] \neq 0, \qquad s \in C_{\text{RHP}}, \qquad 0 \leq \varepsilon \leq 1 \tag{47}$$

A sufficient condition, developed from Eq. (47), guaranteeing the above is

$$\underline{\sigma}[I + K_i(j\omega)G_i(j\omega)] > \bar{\sigma}[K_i(j\omega)\Delta G_i(j\omega)] \quad \text{for } 0 \leq \omega \leq \infty \tag{48}$$

If multiplicative error at $u_i(s)$ is more appropriate [i.e., $u_i = (I + E_i)K_i(y_{i_c} - y_i)$], then $K_i(s)G_i(s, \varepsilon)$ in Eq. (47) must be replaced by $K_i(s, \varepsilon)G_i(s)$, where

$$K_i(s, \varepsilon) = [I + \varepsilon E_i(s)]K_i(s) \tag{49}$$

and another sufficient condition guaranteeing Eq. (47) is

$$\underline{\sigma}[I + \{K_i(j\omega)G_i(j\omega)\}^{-1}] > \bar{\sigma}[E_i(j\omega)] \quad \text{for } 0 \leq \omega \leq \infty \tag{50}$$

The reinterpretation is not that the closed-loop system is guaranteed to be stable, but rather that there is no change in the number of unstable poles. The validity and importance of this step may be unclear at this point, but it will be shown that the requirement in Eq. (47) is an integral part of the stability robustness requirement for the complete feedback loop.

Next, applying Nyquist theory to the true system, after the outer loop closure, yields

$$N_{o_T}(0, \det[I + K_o(s)G'_{o_T}(s)], C_{\text{RHP}}) = Z_{o_T} - P_{o_T} \tag{51}$$

where the notation is consistent with previous analysis. For the block-diagram structure in Fig. 2, $G'_{o_T}(s)$ is defined as

$$G'_{o_T} = G_{o_T}(I + K_i G_{i_T})^{-1} \tag{52}$$

which accounts for modeling errors in both $G_i(s)$ and $G_o(s)$, whereas for the block-diagram structure in Fig. 3, $G'_{o_T}(s)$ is defined as

$$G'_{o_T} = G_{o_T} - G_{oi_T}(I + K_i G_{i_T})^{-1} K_i G_{io_T} \tag{53}$$

which accounts for modeling errors in $G_i(s)$, $G_{io}(s)$, $G_{oi}(s)$, and $G_o(s)$. Again, the requirement

$$Z_{o_T} = 0 \Rightarrow N_{o_T} = -P_{o_T} \tag{54}$$

is necessary for true asymptotic stability of the complete feedback system. Using the notation in Eqs. (19), (42), and (43), P_{o_T} is given as

$$P_{o_T} = P_{K_o} + P_{G'_{o,T}} \tag{55}$$

and the encirclement requirement in Eq. (54) becomes

$$N_{o_T} = -P_{K_o} - P_{G'_{o,T}} \tag{56}$$

Using the standard theory, if 1) the nominal outer closed-loop system is asymptotically stable, or $N_o = -P_{K_o} - P_{G'_o}$ [see Eq. (27)], and 2) the required number of encirclements of the origin is the same for both nominal and true outer closed-loop systems, or $P_{G'_o} = P_{G'_{o,T}}$ [see Eqs. (27) and (56)], then true closed-loop asymptotic stability is guaranteed if

$$\det[I + K_o(s)G'_o(s, \varepsilon)] \neq 0, \qquad s \in C_{\text{RHP}}, \qquad 0 \leq \varepsilon \leq 1 \tag{57}$$

where for the block-diagram structure in Fig. 2, $G'_o(s, \varepsilon)$ is defined as

$$G'_o(s, \varepsilon) = G_o(s, \varepsilon)[I + K_i(s)G_i(s, \varepsilon)]^{-1} \tag{58}$$

whereas for the block-diagram structure in Fig. 3, $G'_o(s, \varepsilon)$ is defined as

$$G'_o(s, \varepsilon) = G_o(s, \varepsilon) - G_{oi}(s, \varepsilon)[I + K_i(s)G_i(s, \varepsilon)]^{-1} \times K_i(s)G_{io}(s, \varepsilon) \tag{59}$$

A sufficient condition guaranteeing Eq. (57) is

$$\underline{\sigma}[I + K_o(j\omega)\tilde{G}'_o(j\omega, \varepsilon)] > \bar{\sigma}[K_o(j\omega)\Delta\tilde{G}'_o(j\omega, \varepsilon)] \quad \text{for } 0 \leq \omega \leq \infty, 0 \leq \varepsilon \leq 1 \tag{60}$$

where for the block-diagram structure in Fig. 2, $\tilde{G}'_o(s, \varepsilon)$ and $\Delta\tilde{G}'_o(s, \varepsilon)$ are defined as

$$\tilde{G}'_o(s, \varepsilon) = G_o(s)[I + K_i(s)G_i(s, \varepsilon)]^{-1} \tag{61}$$

$$\Delta\tilde{G}'_o(s, \varepsilon) = \Delta G_o(s)[I + K_i(s)G_i(s, \varepsilon)]^{-1}$$

whereas for the block-diagram structure in Fig. 3,

$$\tilde{G}'_o(s, \varepsilon) = G_o(s) - G_{oi}(s)[I + K_i(s)G_i(s, \varepsilon)]^{-1} \times K_i(s)G_{io}(s, \varepsilon) \tag{62}$$

$$\Delta\tilde{G}'_o(s, \varepsilon) = \Delta G_o(s) - \Delta G_{oi}(s)[I + K_i(s)G_i(s, \varepsilon)]^{-1} \times K_i(s)G_{io}(s, \varepsilon)$$

If multiplicative error at $u_o(s)$ is more appropriate [i.e., $u_o = (I + E_o)K_o(y_{o_c} - y_o)$], then $K_o(s)G'_o(s, \varepsilon)$ in Eq. (57) must be replaced by $K_o(s, \varepsilon)\tilde{G}'_o(s, \varepsilon)$, where

$$K_o(s, \varepsilon) = [I + \varepsilon E_o(s)]K_o(s) \tag{63}$$

For the block diagram in Fig. 2, $\tilde{G}'_o(s, \varepsilon)$ is defined as

$$\tilde{G}'_o(s, \varepsilon) = G_o(s)[I + K_i(s, \varepsilon)G_i(s)]^{-1} \tag{64}$$

whereas for the block-diagram structure in Fig. 3,

$$\tilde{G}'_o(s, \varepsilon) = G_o(s) - G_{oi}(s)[I + K_i(s, \varepsilon)G_i(s)]^{-1} \times K_i(s, \varepsilon)G_{io}(s) \tag{65}$$

With this, another sufficient condition guaranteeing Eq. (57) is

$$\underline{\sigma}[I + \{K_o(j\omega)\tilde{G}'_o(j\omega, \varepsilon)\}^{-1}] > \bar{\sigma}[E_o(j\omega)]$$

$$\text{for } 0 \le \omega \le \infty, 0 \le \varepsilon \le 1 \tag{66}$$

Although conceptually the same as the standard singular-value robustness tests, Eqs. (60) and (66) are more complicated because of the modeling errors present in more than one location in the feedback system. It would be most desirable to eliminate ε from the tests; unfortunately, this dependence cannot be eliminated in a simple manner (i.e., the singular-value theoretical framework of Refs. 3–5 is not well suited for uncertainties at multiple locations around the loop). However, this is not to say that Eqs. (60) and (66) have no practical value, as will be seen in the next section.

Again, there are practical problems where the inner loop closure around both the nominal and true plants results in destabilization or stabilization of an open-loop mode associated with the outer loop, and this can be accounted for as before with a P^* term. Note, however, that the analysis becomes significantly more complicated (and less useful) if the destabilization or stabilization occurs in the nominal feedback loop but not in the true feedback loop or vise versa. In this situation, the distortion of the Nyquist diagram from the nominal shape to the true shape would be required to pass through the origin exactly P^* times.

To understand how the inner and outer loop adjustable Nyquist diagram requirement relate to that for the complete feedback loop in Fig. 1, consider $\det[I+K(s)G(s, \varepsilon)]$ and the partitioning in Eq. (13). Similar to the development in Eqs. (28–34), $\det[I + K(s)G(s, \varepsilon)]$ can be expressed as

$$\det[I + K(s)G(s, \varepsilon)] = \det[I + K_i(s)G_i(s, \varepsilon)]$$

$$\times \det[I + K_o(s)G'_o(s, \varepsilon)] \tag{67}$$

The result in Eq. (67) is the key to relating the distortion of the Nyquist diagram at each step to the distortion for the complete feedback system. Using Eq. (67), the complete nominal feedback system is robust against modeling errors, as indicated by Eq. (8) if the warpings for the inner and outer loops satisfy Eqs. (47) and (57), respectively. Note that although achieving the individual singular-value robustness requirements in Eqs. (48) and (60), or (50) and (66), implies the requirement in Eq. (8), it does not necessarily imply the requirements in Eqs. (10) and (12), respectively. This is unfortunate in light of the importance and acceptance of measuring multivariable stability robustness with singular values.

However, as a final result, an inequality relationship between the singular values for the overall system and for the inner and outer loops is given, which holds only for the feedback structure in Fig. 2 Using Eq. (15), the return difference for the overall system can be rewritten as the product of the return differences for the inner and outer loop closures, or

$$I + KG = (I + K_oG'_o)(I + K_iG_i) \tag{68}$$

Taking the singular value of Eq. (68) and using singular-value inequality relationships leads to

$$\underline{\sigma}[I + KG] \ge \underline{\sigma}[I + K_iG_i]\underline{\sigma}[I + K_oG'_o] \tag{69}$$

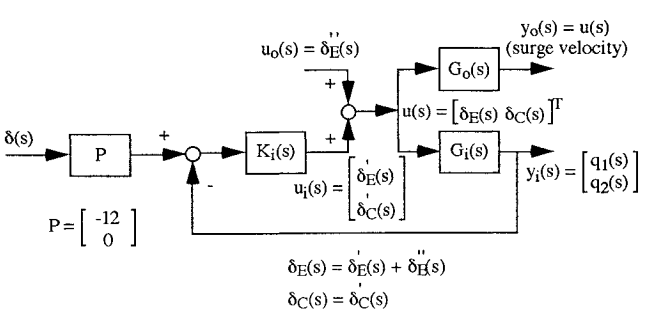

Fig. 6 Inner loop block diagram.

Equation (68) can be rewritten as

$$KG[I + (KG)^{-1}] = [I + (KG)^{-1}]KG$$

$$= K_oG'_o[I + (K_oG'_o)^{-1}][I + (K_iG_i)^{-1}]K_iG_i \tag{70}$$

and manipulation of Eq. (70) leads to

$$\underline{\sigma}[I + (KG)^{-1}] \ge \frac{\underline{\sigma}[K_iG_i]\underline{\sigma}[K_oG'_o]}{\bar{\sigma}[KG]}$$

$$\times \underline{\sigma}[I + (K_iG_i)^{-1}]\underline{\sigma}[I + (K_oG'_o)^{-1}] \tag{71}$$

Example

The example to be considered involves the longitudinal flight control of a large, flexible aircraft. Controlled inputs consist of elevator deflection δ_E and canard deflection δ_C (both in radians), whereas responses of interest include the pitch rate measured at two locations on the fuselage, q_1 and q_2 (in radians per second) and the surge velocity u (in feet per second). The model for the aircraft dynamics is 12th order and the state-space description is given in Ref. 17. The flight control design objectives are to increase the damping of the short period and aeroelastic modes, reduce the aeroelastic contributions to the pitch rate responses, and stabilize the phugoid mode (one right-half plane pole). With the existing frequency separation between the phugoid mode and the other modes, the flight control synthesis will be accomplished in a two-step approach, as indicated in Fig. 2. The inner loop closure consists of angular rates q_1 and q_2 fed back to δ_E and δ_C, respectively, whereas the outer loop closure consists of speed u fed back to δ_E.

The inner loop compensation was synthesized in Ref. 26 and is briefly reviewed here. First, the q_2/δ_C loop is closed to improve the first aeroelastic mode damping. Next, a δ_E-to-δ_C crossfeed is introduced to reduce first aeroelastic mode excitations from δ_E. Finally, the q_1/δ_E loop is closed to improve the short-period damping. A notch filter is introduced at 11 rad/s to reduce the effects from the second aeroelastic mode, whereas a low pass-filter with a bandwidth of 60 rad/s is included for attenuation of higher frequency aeroelastic modes. With this, the inner loop compensator is

$$K_i(s) = \frac{60}{s+60}\,\frac{s^2+0.47s+116}{s^2+3.2s+116}\begin{bmatrix}-0.05 & 0\\ 0.075 & 0.05\end{bmatrix} \quad \text{(rad/rad/s)} \tag{72}$$

and the block-diagram structure is shown in Fig. 6, where δ represents the pilot stick inputs.

For this loop closure, $P_{K_i} = 0$ and $P_{G_i} = 0$ since stabilization of the phugoid mode is not an objective of the inner loop closure. The Nyquist diagram corresponding to $\det[I + K_iG_i]$ is shown in Fig. 7 and note that $N_i = 0$ indicating the inner loop nominal stability requirement is satisfied [see Eq. (23)].

Suppose here that modeling errors for the inner loop consist of generic time delay at $u_i(s)$, or

$$E_i(s) = (e^{-\tau_i s} - 1)I \tag{73}$$

To assess the "stability robustness," the inner loop singular-value test is plotted in Fig. 8. From Fig. 8 observe that Eq. (50) is satisfied and "robustness" is assured for $\tau_i \le 0.25$ s.

Now, the outer loop consists of constant-gain feedback of speed u, or

$$K_o(s) = 0.0001 \text{ rad/ft/s} \tag{74}$$

and the block diagram is shown in Fig. 9. Here, $P_{K_o} = 0$ and $P_{G'_o} = 1$ due to the leftover phugoid instability from the inner loop closure. The Nyquist diagram corresponding to $\det[I + K_oG'_o]$ is shown in Fig. 10, and it is seen that $N_o = -1$, indicating the phugoid mode has been stabilized and Eq. (27) is satisfied.

For the outer loop, generic time delay at $u_o(s)$ is considered as the modeling error, or

$$E_o(s) = e^{-\tau_o s} - 1 \tag{75}$$

To assess the stability characteristics in the presence of $E_o(s)$ only, the singular-value test for the outer loop closure with $\varepsilon = 0$ is plotted in Fig. 11. From Fig. 11 note Eq. (66), with $\varepsilon = 0$, is satisfied for $\tau_o \leq 6$ s. However, to assure robustness in the presence of both $E_o(s)$ and $E_i(s)$, $\varepsilon \neq 0$ must be considered. Rather than plotting multiple curves corresponding to $\underline{\sigma}[I + (K_o\tilde{G}_o')^{-1}]$ for each value of ε, only a single curve is plotted that gives the lower bound on $\underline{\sigma}[I + (K_o\tilde{G}_o')^{-1}]$, as ε is ranged from 0 to 1. From Fig. 11 note Eq. (66) is satisfied for all appropriate ε and robustness is

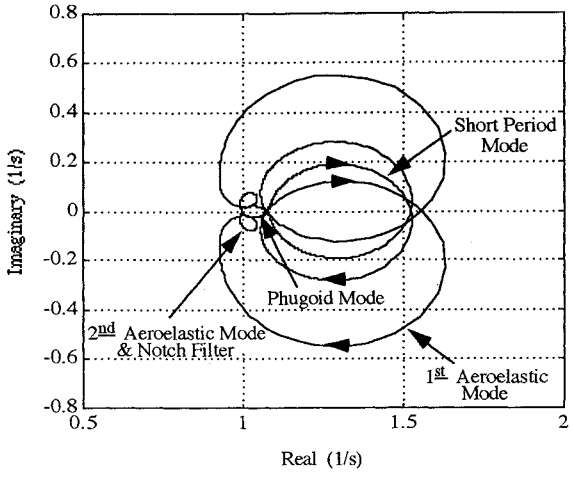

Fig. 7 Inner loop Nyquist diagram.

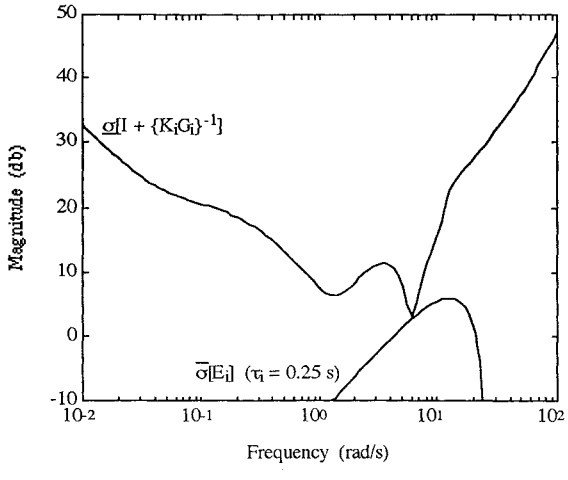

Fig. 8 Inner loop singular-value robustness trace.

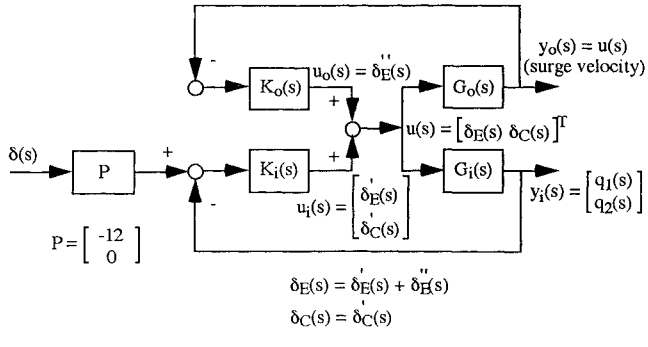

Fig. 9 Inner and outer loop block diagram.

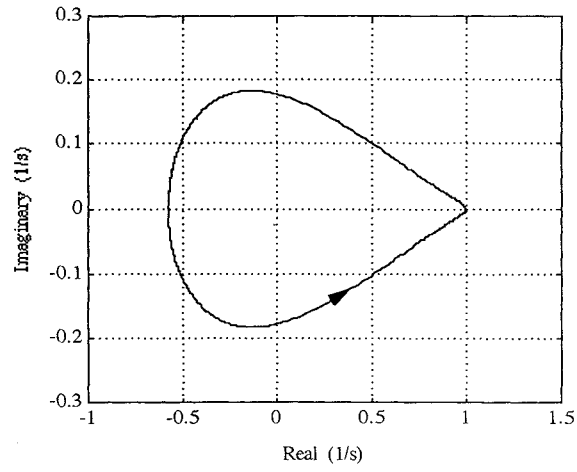

Fig. 10 Outer loop Nyquist diagram.

assured for $\tau_o \leq 6$ s and $\tau_i \leq 0.25$ s. Observe the small change in $\underline{\sigma}[I + (K_o\tilde{G}_o')^{-1}]$ above 1 rad/s for nonzero values of ε.

Although finished with a first attempt for the sequential design, the flight control engineer is now faced with questions concerning how the stability and stability robustness results at the inner and outer loop closures contribute to the overall system properties, and if not satisfactory, what modifications to the sequential design should be implemented. This is where the results developed in previous sections are appropriate.

For example, uncertainty might exist as to the role the intermediate encirclement requirement plays in the overall encirclement requirement, since the final loop closure is what stabilizes the phugoid mode. Equation (35) indicates that the intermediate encirclement requirement ($N_i = 0$) does not contribute to the overall requirement. A "picture" of this is shown in Fig. 12, where the Nyquist diagram corresponding to the complete feedback system or $\det[I + KG]$ is plotted, along with the results from Figs. 7 and 10. Observe how the inner loop Nyquist diagram does not contribute to the origin encirclement, leaving the outer loop Nyquist diagram to "unwrap" the origin and stabilize the phugoid mode.

TWAs another example, it has been argued in the technical literature that stability robustness of the overall closed-loop system with all feedback loops broken simultaneously and all uncertainties considered together is the key characteristics to consider, rather than analysis based upon breaking one loop at a time with one uncertainty present.[3-5] The flight control engineer should be interested in how the robustness properties at the inner and outer loop closures contribute to this characteristic and Eq. (71) aids in this task. Figure 13 shows the singular-value robustness of the complete system, or $\underline{\sigma}[I + (KG)^{-1}]$, along with the right-hand side of Eq. (71). Note how the inner and outer loop characteristics shape the overall system characteristic. If the overall singular-value trace needs to be shaped slightly different to provide a satisfactory system, the flight control engineer now has insight concerning where to make modifications in the sequential design. After becoming exposed to and familiar with the new results presented, it is possible for the flight control engineer to anticipate the consequences of his current loop closure upon the overall system properties, evaluated "downstream" in the design process.

Figure 13 also shows the inner and outer singular-value characteristics from Figs. 8 and 11. Observe how the inner and outer loop singular-value traces match the high- and low-frequency range, respectively, of the trace corresponding to the overall system. This is a special result due to the type -1 inner loop (see Fig. 5).[17] In the high-frequency range (above 0.15 rad/s) K_oG_o' is attenuated relative to I and Eq. (70) becomes $[I + (KG)^{-1}](KG) \approx [I + (K_iG_i)^{-1}]K_iG_i$, leading to, for high frequencies,

$$\underline{\sigma}[I + (KG)^{-1}] \approx \underline{\sigma}[I + (K_iG_i)^{-1}] \tag{76}$$

For low frequencies (below 0.15 rad/s), K_iG_i is attenuated relative to I, and Eq. (70) becomes $KG[I + (KG)^{-1}] \approx K_oG_o'[I + (K_oG_o')^{-1}]$,

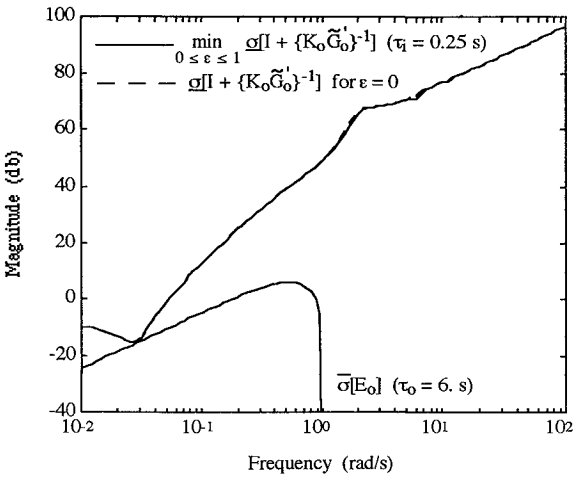

Fig. 11 Outer loop singular-value robustness trace.

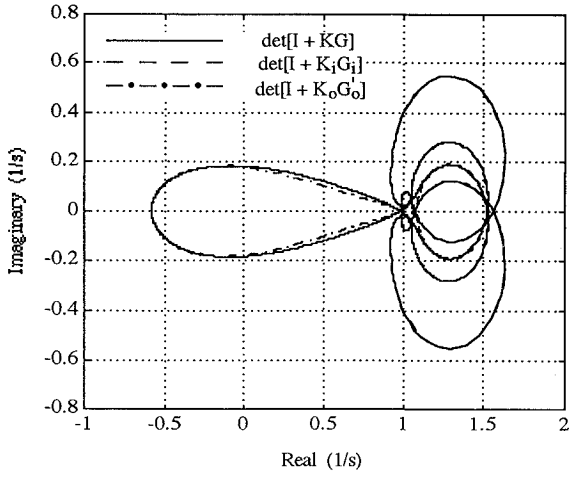

Fig. 12 Nyquist diagram comparisons.

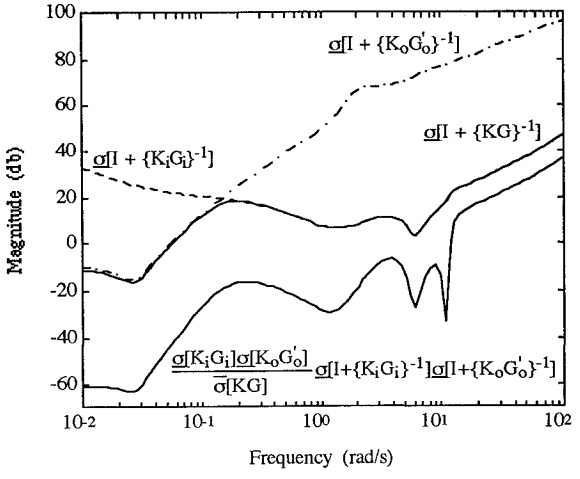

Fig. 13 Singular value robustness trace comparisons.

yielding, for low frequencies,

$$\underline{\sigma}[I + (KG)^{-1}] \approx \underline{\sigma}[I + (K_oG_o')^{-1}] \tag{77}$$

Here, the flight control engineer has obtained still more insight into the contributions to the overall system characteristics from the inner and outer loop closure design steps.

As a final result, recall that the distance from the origin to the nominal Nyquist diagram can be used as a measure of stability robustness. Therefore, Eq. (67) with $\varepsilon = 0$ and Fig. 12 also indicate the contributions to the overall robustness from the intermediate and final steps. Again observe the close match between the inner and outer loop contours with the high- and low-frequency segments of the overall contour, respectively. This offers useful insight as well.

Conclusions

It has been shown how the nominal, multivariable Nyquist diagram and its continuous warping to the true shape for the overall feedback system is related to the contributions from the inner and outer loops. The encirclement requirement of the overall feedback system to assure nominal asymptotic stability is converted to the encirclement requirements for the inner and outer loops. Further, to assure robustness against modeling errors, the requirement of avoiding the origin, when the Nyquist diagram is warped from the nominal shape to the true shape, is converted to similar requirements for the inner and outer loops. The implications for analysis and design are that the overall stability and robustness characteristics can be decomposed into contributions from the inner and outer loops, which can offer guidance during feedback design.

Acknowledgments

This research was supported by NASA Langley Research Center under Grant NAG1-758. D. Arbuckle served as technical monitor.

References

[1]Nyquist, H., "Regeneration Theory," *Bell System Technical Journal*, Vol. 11, 1932, pp. 126–147.

[2]MacFarlane, A. G. J., and Postlethwaite, I., "The Generalized Nyquist Stability Criterion and Multivariable Root Loci," *International Journal of Control*, Vol. 25, No. 1, 1977, pp. 81–127.

[3]Doyle, J. C., and Stein, G., "Multivariable Feedback Design: Concepts for a Classical/Modern Synthesis," *Transactions on Automatic Control*, Vol. AC-26, No. 1, 1981, pp. 4–16.

[4]Lehtomaki, N. A., Sandell, N. R., and Athans, M., "Robustness Results In Linear-Quadratic Gaussian Based Multivariable Control Designs," *Transactions on Automatic Control*, Vol. AC-26, No. 1, 1981, pp. 75–92.

[5]Lehtomaki, N. A., "Practical Robustness Measures in Multivariable Control System Analysis," Ph.D. Dissertation, Dept. of Electrical Engineering and Computer Science, Massachusetts Inst. of Technology, Cambridge, MA, May 1981.

[6]McRuer, D., Ashkenas, I., and Graham, D., *Aircraft Dynamics and Automatic Control*, Princeton Univ. Press, Princeton, NJ, 1973.

[7]Maciejowski, J. M., *Multivariable Feedback Design*, Addison-Wesley, Reading, MA, 1989.

[8]Kokotovic, P. V., O'Malley, R. E., and Sannuti, P., "Singular Perturbations and Order Reduction in Control Theory: An Overview," *Automatica*, Vol. 12, No. 2, 1976, pp. 123–132.

[9]Saksena, V. R., O'Reilly, J., and Kokotovic, P. V., "Singular Perturbations and Time-Scale Methods in Control Theory: Survey 1976–1983," *Automatica*, Vol. 20, No. 3, 1984, pp. 273–293.

[10]Chow, J. H., and Kokotovic, P. V., "A Decomposition of Near-Optimum Regulators for Systems with Slow and Fast Modes," *Transactions on Automatic Control*, Vol. AC-21, No. 10, 1976, pp. 701–705.

[11]Khalil, H. K., "On the Robustness of Output Feedback Control Methods to Modeling Errors," *Transactions on Automatic Control*, Vol. AC-26, No. 2, 1981, pp. 524–526.

[12]Calise, A. J., Prasad, J. V. R., and Siciliano, B., "Design of Optimal Output Feedback Compensators in Two Time Scale Systems," *Transactions on Automatic Control*, Vol. AC-35, No. 4, 1990, pp. 488–492.

[13]Porter, B., and Shenton, A. T., "Singular Perturbation Analysis of the Transfer Function Matrices of a Class of Multivariable Linear Systems," *International Journal of Control*, Vol. 21, No. 4, 1975, pp. 655–660.

[14]Luse, D. W., and Khalil, H. K., "Frequency Domain Results for Systems with Slow and Fast Dynamics," *Transactions on Automatic Control*, Vol. AC-30, No. 12, 1985, pp. 1171–1178.

[15]Khalil, H. K., "Output Feedback Control of Linear Two Time Scale Systems," *Proceedings of the American Control Conference*, Boston, Massachusetts, June, 1985, pp. 1397–1400.

[16]Khalil, H. K., "Output Feedback Control of Linear Two-Time-Scale Systems," *Transactions on Automatic Control*, Vol. AC-32, No. 9, 1987, pp. 784–792.

[17]Newman, B., and Schmidt, D. K., "A Sequential Approach to Multivariable Stability Robustness Analysis," *Proceedings of the AIAA Guidance, Navigation, and Control Conference*, AIAA, Washington, DC, 1991, pp. 1510–1518.

[18]Hsu, C., and Chen, C., "A Proof of the Stability of Multivariable Feedback Systems," *Proceedings of the IEEE*, Vol. 56, No. 11, 1968, pp. 2061–2062.

[19]Churchill, R. V., and Brown, J. W., *Complex Variables and Applications*, McGraw-Hill, St. Louis, MO, 1984.

[20]Blakelock, J. H., *Automatic Control of Aircraft and Missiles*, Wiley, New York, 1965.
[21]Stevens, B. L., and Lewis, F. L., *Aircraft Control and Simulation*, Wiley, New York, 1992.
[22]McLean, D., *Automatic Flight Control Systems*, Prentice-Hall, London, 1990.
[23]McRuer, D. T., Myers, T. T., and Thompson, P. M., "Literal Singular-Value-Based Flight Control System Design Techniques," *Journal of Guidance, Control, and Dynamics*, Vol. 12, No. 6, 1989, pp. 913–919.
[24]McRuer, D., "Progress and Pitfalls in Advanced Flight Control Systems," *Advances in Guidance and Control Systems, AGARD Conference Proceedings No. 321*, Lisbon, Portugal, October, 1982, pp. K1–K17.
[25]McRuer, D., Johnston, D., and Myers, T., "A Perspective on Super-augmented Flight Control Advantages and Problems," *Active Control Systems: Review, Evaluation and Projections, AGARD Conference Proceedings* No. 384, Toronto, Canada, October, 1984, pp. 3.1–3.16.
[26]Newman, B., and Schmidt, D. K., "Aeroelastic Vehicle Multivariable Control Synthesis with An Analytical Robustness Evaluation," *Journal of Guidance, Control, and Dynamics*, Vol. 18, No. 1, January–February, 1995.
[27]Nobel, B., and Daniel, J. W., *Applied Linear Algebra*, Prentice-Hall, Englewood Cliffs, NJ, 1977.
[28]Ogata, K., *Modern Control Engineering*, Prentice-Hall, Englewood Cliffs, NJ, 1970.